Thermo-elastic Response of Cutaneous and Subcutaneous Tissues to Noninvasive Radiofrequency Heating

Joel N. Jimenez-Lozano[1], Paulino Vacas-Jacques[1] and Walfre Franco[*1],
[1] Wellman Center for Photomedicine, Massachusetts General Hospital, Harvard Medical School
*40 Blossom St, Boston, MA, 02114, wfranco@partners.org

Abstract: Radiofrequency (RF) technology offers unique advantages for noninvasive selective heating of relatively large volumes of tissue. In this work, we present a mathematical model for selective non-invasive, non-ablative RF heating of cutaneous and subcutaneous tissue (with detailed fiber septa structures) including their thermo-elastic response. Our analysis shows that the fiber septa architecture affect the static electric field within subcutaneous fat. There is greater electric power absorption in the fiber septa filaments than in fat and it favors the flux of electric current density. When reaching the thermal steady-state, fiber septa contributes to enhance the selective heating of subcutaneous fat tissue. Fiber septa shows shrinkage due to its thermoelastic response, agreeing with clinical observations.

Keywords: skin, radiofrequency heating, bioheat transfer, thermoelastic, hyperthermia.

1. Introduction

Radiofrequency energy exposure is a well-established method for generating heat in tissue to incise, excise, ablate or coagulate the targeted tissue. There exist mainly two types of RF devices for cutaneous applications, monopolar and bipolar. Monopolar systems deliver current through a single contact point (electrode) with a grounding pad (return) for current flow to complete the electrical circuit. Bipolar devices only pass electrical current between two positioned electrodes, no grounding pad is necessary. RF has gained popularity because of its noninvasive nature and the capability of selectively heat target tissues without injuring surrounding tissue. Dermal morphology is a combination of collagen fibers with pockets of fats and fluids trapped within this fibrous mesh structure. There is a lack of understanding around the physical electro-thermo-elastic mechanism of dermal heating by the presence of the fiber septa network interlaced between fat lobules and its qualitative and quantitative features.

The objectives of this work are to (i) present a mathematical model for selective, non-invasive, non-ablative RF heating of cutaneous and subcutaneous tissue including their thermo-elastic response; (ii) investigate the effect of fiber septa networks interlaced between fat locules in the RF energy deposition; (iii) illustrate the physical electric, thermal and elastic outcomes; (iv) discuss the implications for the clinical use.

2. Problem Description

2.1 Governing Equations

Biological tissue is an electrically conducting media for which the *static electric field* $E_i = -\nabla V_i$ can be obtained from

$$\nabla \cdot (\sigma_i \nabla V_i) = 0, \tag{1}$$

where σ is the electric conductivity in (S/m), V≡V(x,y) is the voltage in (volts) dependent of space (x,y). (x,y) are the lateral and depth coordinates, respectively, and the subindex i represents the skin, subcutaneous fat, muscle, or fiber septa $i=\{s,f,m,sp\}$, respectively. The rate of energy dissipated per unit volume at a given point is directly proportional to the electric conductivity of the tissue and to the square of the induced internal electric field, $Q_i = \sigma_i \|E_i\|^2/2$, where Q is the power absorption in (W/m^3) and E is the electric field in (V/m).

The *bioheat transfer* equation in tissue including thermo-elastic coupling is given by

$$\rho_i c_i \frac{\partial T_i}{\partial t} + \alpha_i T_0 \frac{\partial (\bar{\sigma}_{kk})_i}{\partial t} = \nabla \cdot (k_i \nabla T_i) + c_b \omega_i (T_b - T_i) + Q_i, \tag{2}$$

where ρ is the density of the tissue in (kg/m^3), c is the specific heat of the tissue in (J/kg/K), t is the time in (s), T≡ T(x,y,t) is the temperature in (K), k is the thermal conductivity in (W/m/K), ω_b is the blood perfusion rate in (kg/m^3/s), c_b is the blood specific heat in (J/kg/K), T_b is the arterial temperature in (K), α is the thermal expansion coefficient in (1/K), T_0 is the initial temperature in (K) and $\bar{\sigma}$ is the stress ($_{kk}$ subindices indicate the trace of the stress tensor) in (Pa).

The *motion equation* for an isotropic linear elastic solid

$$\rho_i \frac{\partial^2 \boldsymbol{u}_i}{\partial t^2} - \overline{\nabla} \cdot \bar{\sigma}_i = \overline{F}_i, \tag{3}$$

where $\boldsymbol{u}$ ={u,v} is the displacement vector in (m), $\bar{\sigma}$ is the stress tensor in (Pa), $\overline{F}_v$, are external volume forces in (Pa/m^2). Constitutive relations for an isotropic linear elastic material are: (i) The stress tensor $\bar{\sigma} = [\boldsymbol{S} \cdot (\boldsymbol{I} + \overline{\nabla}\boldsymbol{u})]$, where $\boldsymbol{S}$ is the Duhamel term which relates the stress tensor to the strain tensor and temperature, $\overline{\nabla}\boldsymbol{u}$ is the displacement gradient and $\boldsymbol{I}$ is an identity matrix; (ii) The Duhamel relation $\boldsymbol{S} - \boldsymbol{S}_0 = \boldsymbol{C}: (\bar{\epsilon} - \alpha(T - T_0) - \bar{\epsilon}_0)$, where $\boldsymbol{C}$ is the stiffness tensor and depends on the elastic Young's modulus, E; and the Poisson's ratio, ν; (iii) The strain tensor $\bar{\epsilon} = [\overline{\nabla}\boldsymbol{u}^T + \overline{\nabla}\boldsymbol{u}]/2$. The formulation of elasticity equations is Lagrangian. They are derived in a material frame of reference in a coordinate system **X**≡(X,Y). When solid objects deform due to external or internal forces and constraints, each material particle keeps its coordinates **X**≡(X,Y), while spatial coordinates **x**≡(x,y) change with time and applied forces such that it follows a path **x**≡**X**+ $\boldsymbol{u}$ (**X**,t) in space. The operator $\overline{\nabla}$ is computed with respect to the material coordinates. Electric propagation is assumed time independent since it is very fast compared to heat diffusion and thermo-elastic response. Note that we are using a quasi-static electric approximation. In the quasi-static approximation the characteristic length of the object of study is much less than the wavelength of the electromagnetic (EM) field: skin thickness is ~0.002 meters and the wavelength at 1 MHz is 300 meters. A quasi-static approach means that the spatial distribution of the EM fields over the extent of the device is the same as that of static fields. Electric, thermal, elastic and perfusion properties are assumed constant and temperature independent, Table 1. Electrical properties are frequency dependent, those used herein correspond to 1 MHz. However, the electric conductivity remains fairly constant for frequencies from 10^3 to 10^6 Hz and the permittivity decreases by one order of magnitude in the same frequency range [1]. The perfusion term in the septa is neglected, ω_{sp}=0. Within a temperature range of (38 to 45 ^{o}C), variations in specific heat, thermal conductivity and blood perfusion are not significant [2,3]. We have assumed that tissue behaves as an isotropic linear elastic material. Strains and displacements are small, their elastic properties are not dependent on the direction and can be characterized by their Young's modulus and Poisson's ratio. Electrical and thermal properties of fiber septa bundles are assumed to be similar to those of the dermis.

2.2 Domain, Boundary and Initial Conditions

Domain. Consider three layers of tissue --- skin, fat and muscle --- as shown in Fig. 1. Each layer has a known thickness l_i. The domain of study is W *x* L_t, where W is the total width and L_t=l_s+l_f+l_m is the total depth. Cutaneous and subcutaneous tissues are commonly considered layered structures in terms of RF energy deposition. This is a valid assumption for cutaneous tissues, namely epidermis and dermis. However, the subcutaneous structure of tissue consists of a fine collagen fiber mesh (interlaced fiber septa) with clusters of adipocytes. The specific anatomical structure of septa within subcutaneous fat tissue *in vivo* has been studied using micro magnetic resonance imaging (Micro-MRI) [4]. Micro-MRI can clearly show the thickness and the structural alterations of the connective tissue in the dermis and the subcutaneous fat cells in the hypodermis correlated with abnormalities of the skin. For investigation purposes we have selected a specific geometry of septa configuration which was shown to be correlated to cellulite presence in human subjects, see Fig. 2. In order to get a realistic fiber septa configuration, we post-processed the published Micro-MRI Images using Adobe Illustrator CS3 (Adobe Systems Inc.) and produce an importable file with the geometric data.

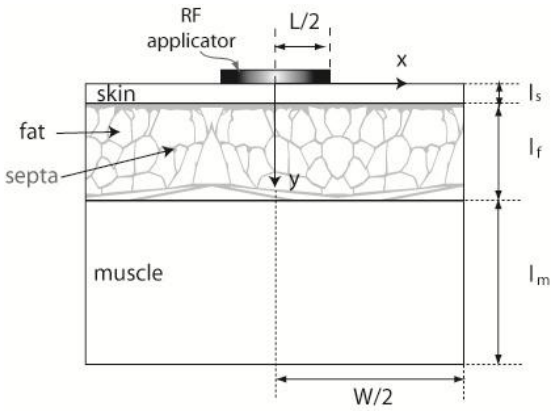

Figure 1. Tissue layers of skin, fat, muscle, fiber septa bundles and RF applicator. Mathematical domain: $-W/2<x<W/2$ and $0<y<(l_s+l_f+l_m)$.

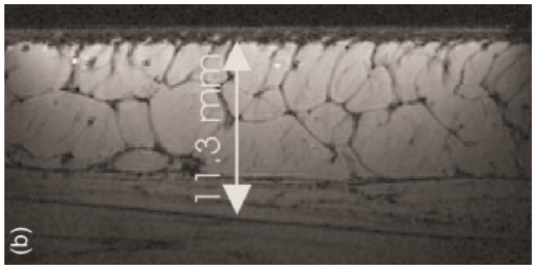

Figure 2. High-resolution *in vivo* MRI of the skin of a female [4]. Dark filaments correspond to fiber septa within the subcutaneous fat.

Boundary and Initial Conditions. The voltage distribution beneath RF applicators is commonly known [5,6]. The RF applicator is modeled as a constant voltage source at the skin surface with a known size extension L. We used an empirical voltage distribution as given in Franco, W. et al. [6] for a monopolar applicator, $V(-L \le x \le L) = [a\left(\frac{lx}{L}\right)^2 + b]\sqrt{PZ}$, where a = 1.28, b = $-2.25\text{x}10^{-3}$, P is the applied RF power in watts and Z the impedance of the tissues in ohms. The electric, thermal and elastic governing equations for each region are given by Eqs. (1)--(3). Boundary conditions are the following: (a) *electrical*, the RF applicator is modeled as a spatially-dependent voltage source distribution at the skin surface, a zero voltage condition at the muscle end and no electric flux at the outer boundaries; (b) *thermal*, underneath the applicator a cooling plate at temperature T_{plate} is mounted and air convection to the surrounding environment at the sides of the applicator, T_∞; (c) *elastic*, fixed conditions at the skin outer surface and muscle end, and outer lateral boundaries are assumed to move freely. There is no thermal and electrical resistance between layers. As initial conditions at t=0 s, we assume V=0, T_0=310 K and no strain.

3. Numerical Solution

Finite element analysis (COMSOL Multiphysics, Burlington, MA, USA) was used to solve our mathematical model. Using COMSOL 4.1, the model was implemented using the electric currents, heat transfer and solid mechanics modules. Simulations were ran in a Intel Core i5 at 3.1 GHz PC computer with 4 GB RAM memory. The model in total has 355,772 degrees of freedom. Processing the full model requires about 134 min real time. The model mesh consists of 44380 elements. Skin, fat, muscle and septa central domains had a higher mesh density. The time dependent solution was set from 0-1200 seconds with a time-step of 0.1 seconds. We used COMSOL MUMPS direct solver.

4. Results

4.1 Voltage Distribution and Electric Power Absorption

Skin, fat and muscle tissues are dielectric materials that can be polarized by an electric field. The applied voltage produces an electric field that points from regions of high to low potential. Voltage distributions within skin, fat and muscle are shown in Fig. 3 and Fig. 4. For comparison we have studied the conditions of subcutaneous fat as homogeneous tissue (Fig. 3) and with high density of fiber septa (Fig. 4). Voltage drop occurs mostly within skin and fat layers. Internal voltage distributions bear similarity to the surface voltage distributions established by the RF applicator (quadratic function), having their maximum value located below the maxima of the surface distribution, as shown in Fig. 3 and Fig. 4. The presence of fiber septa alters the voltage distribution form within tissue.

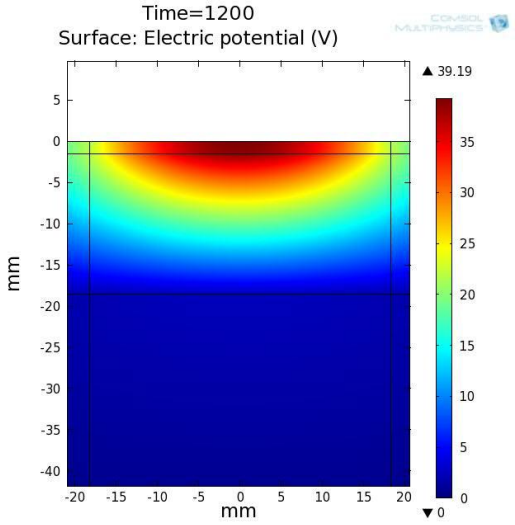

Figure 3. Voltage distribution within tissue, homogeneous fat tissue (no fiber septa).

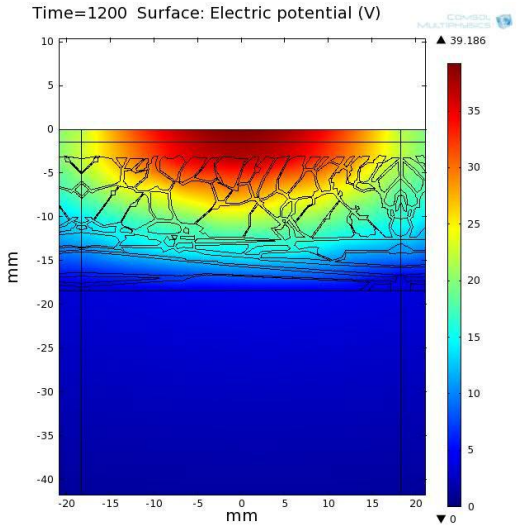

Figure 4. Voltage distribution within tissue, fat tissue with high density of fiber septa.

For the selected voltage distribution of the RF applicator, the electric flux in skin is greater resulting in accumulation of power absorption beneath the applicator edges, see Fig.5. Fiber septa favors the flow of the electric flux and causes higher accumulation in some fibers when compared to the skin-applicator edges. The power absorption in the case of high density fiber septa is shown in Fig. 6.

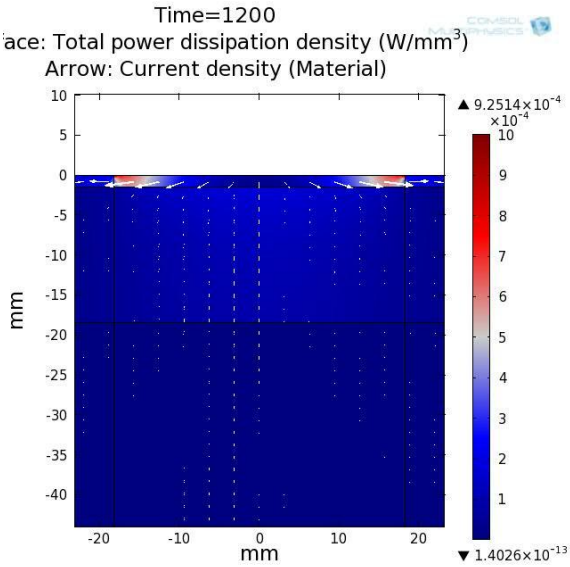

Figure 5. Electric power absorption and Electric field (arrows) within tissue for homogeneous fat tissue.

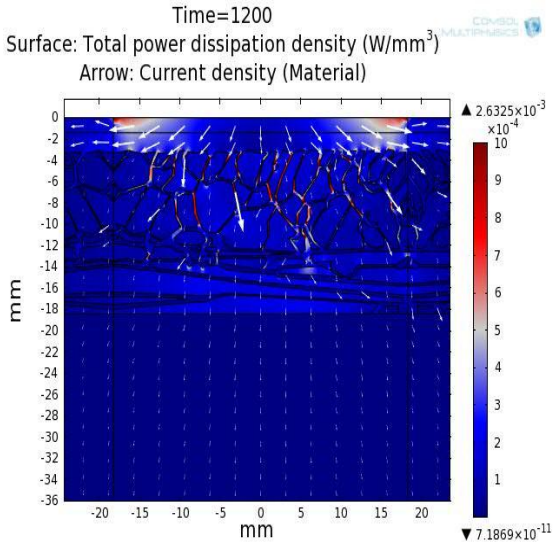

Figure 6. Electric power absorption (surface map) and Electric field (Arrows) within tissue for fat with high density of fiber septa.

4.2 Temperature

Selective heating of subcutaneous fat and fiber septa is due to the total absorbed electric power, results at t=30 seconds are shown in Fig. 7. Steady-state heat diffusion is reached around 1200 seconds (20 minutes). The steady-state temperature map for homogeneous subcutaneous fat tissue is shown in Fig. 8. We observe a confinement of heat in the fat region with a

maximum temperature of 326.32 K. Heat confinement is a consequence of relatively low energy absorption by skin at the applicator center and heat diffusion from the adjacent skin into the fat. The contribution of fiber septa is to enhance heat distribution due to their complementary selective heating. Higher temperatures are reached within the subcutaneous fat, see Fig. 9. Maximum temperatures is 334.47 K for fat with high density fiber septa. This shows a ~8 degrees Celsius difference.

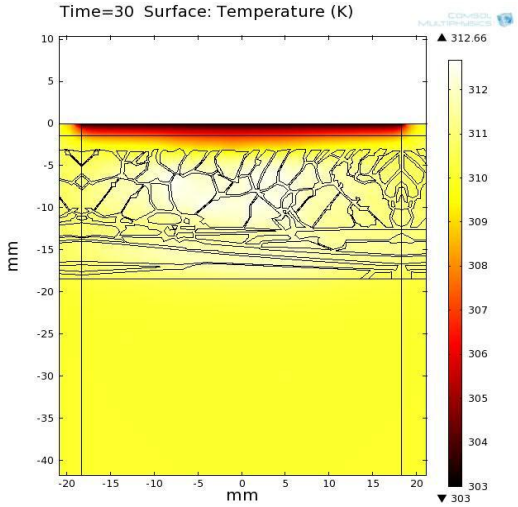

Figure 7. Temperature map at 30 seconds for fat tissue with high density of fiber septa.

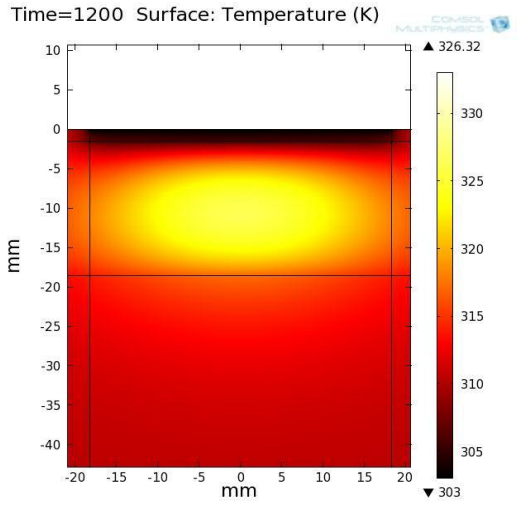

Figure 8. Temperature map at 1200 seconds (steady-state) for homogeneous fat tissue.

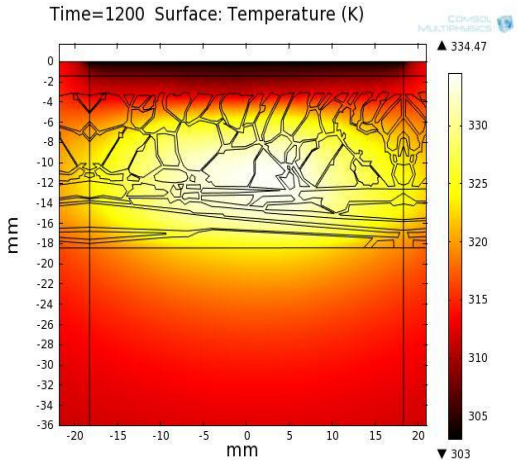

Figure 9. Temperature map at 1200 seconds (steady-state) for fat tissue with high density of fiber septa.

4.3 Strain

Volumetric strain can be used to measure the thermo-elastic response of the tissue. During the initial strain most of the subcutaneous tissue, including septa has a positive value of strain showing that is initially expanding before heat diffusion is completed, as shown in Fig. 10. Skin has a negative strain due to the low temperature relative to the initial unstrained bulk reference temperature. At the steady-state, overall fiber septa has a negative strain (shrinkage) but near to the high temperature region it gains positive values of strain, see Fig. 11.

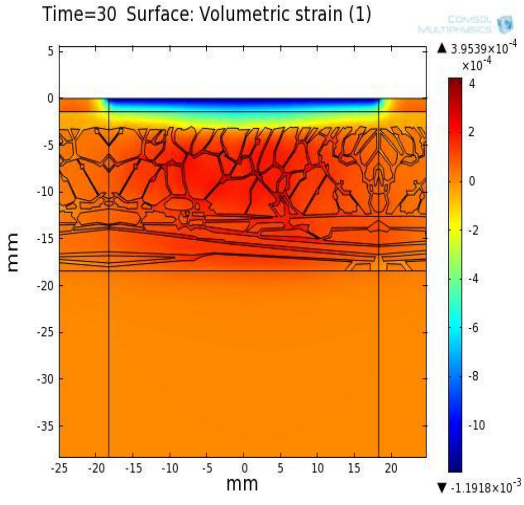

Figure 10. Volumetric strain at 30 seconds for the high density fiber septa.

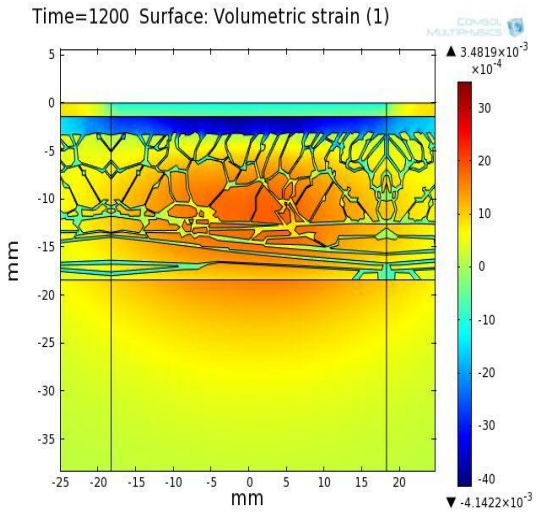

Figure 11. Volumetric strain at steady-state for the high density fiber septa.

5. Discussion

We have showed that fiber septa structures in the subcutaneous fat tissue have an important role in the transient and steady-state thermal states as well as in the elastic response of the tissue. These results are important to the field of clinical hyperthermia. An specific clinical application of our analysis is in the hyperthermic injury of adipocyte cells. Results can be helpful in the clinical treatment of subcutaneous fat related disorders, such as, lipomatosis, Madelung's disease, or lipedema. MRIs of lipedema show massive circumferential enlargement of the subcutaneous tissue occupied by fat lobules and a highly dense fibrous septa structure [7]. The literature reports that adipocyte cells are heat sensitive to 50^{o}C for 1 min and 42–45^{o}C for 15 min thermal exposures, which result in delayed cellular death response [5,6]. Treatments protocols can be designed under short exposure, high power on-off cycles or long exposure, low power modes to provide lethal localized hyperthermic injury in the subcutaneous tissues. Other applications are in the aesthetic field for tissue tightening, wrinkle reduction, pore reduction, among others [8].

6. Conclusions

We presented and solved a mathematical model for selective non-invasive, non-ablative RF heating of cutaneous and subcutaneous tissue (with detailed fiber septa structures) including their thermo-elastic response. Our analysis shows that the presence of the fiber septa architecture contributes to change the static electric field within subcutaneous fat. There is greater electric power absorption in the fiber septa filaments and favors the flux of electric current density. When reaching the thermal steady-state, fiber septa contributes to enhance selective heating of subcutaneous fat tissue. Fiber septa shows shrinkage due to thermo-elastic response. RF hyperthermia can be used to treat subcutaneous fat diseases and to enhance therapeutic strategies due to a better understanding of the involved physics.

7. References

1. D. Miklavcic, N. Pavselj, and F. X. Hart. Electric Properties of Tissues. *Wiley Encyclopedia of Biomedical Engineering* (2006).
2. D. Haemmerich, D. J. Schutt, J. G. Webster I. dos Santos, and D. M. Mahvi. Measurement of temperature-dependent specific heat of biological tissues. *Physiological Measurement*, **26(1)**: 59–67 (2005).
3. F. Xu, T. J. Lu, K. A. Seffen, and E. Y. K. Ng. Mathematical modeling of skin bioheat transfer. *Applied Mechanics Reviews*, **62**, 050801–1–050801–35 (2009).
4. F. Mirrashed, J. C. Sharp, V. Krause, J. Morgan, and B. Tomanek, Pilot study of dermal and subcutaneous fat structures by MRI in individuals who differ in gender, BMI, and cellulite grading, *Skin Research and Technology*, **10**, 161-168 (2004).
5. W. Franco, A. Kothare, and D. J. Goldberg. Controlled volumetric heating of subcutaneous adipose tissue using a novel radiofrequency technology, *Lasers in Surgery and Medicine*, **41**,745–750 (2009).
6. W. Franco, A. Kothare, S. J. Ronan, R. C. Grekin, and T. H. McCalmont. Hyperthermic injury to adipocyte cells by selective heating of subcutaneous fat with a novel radiofrequency

device: Feasibility studies, *Lasers in Surgery and Medicine*, **42**, 361–370 (2010).
7. M. A. Fonder, J. W. Loveless, and G. S. Lazarus, Lipedema, a frequently unrecognized problem, *J Am Acad Dermatol*, **57(2)**, S1-S3 (2007).
8. M. T. Abraham and E. V. Ross, Current concepts in non-ablative radiofrequency rejuvenation of the lower face and neck, *Facial Plastic Surgery*, **21(1)**, 65-73 (2005).
9. C. Pailler-Mattei, S. Bec and H. Zahouani, In vivo measurements of the elastic mechanical properties of human skin by indentation tests, *Medical Engineering & Physics*, **30**, 599-606 (2008).
10. K. Comley and N. A. Fleck, A micromechanical model for the Young's modulus of adipose tissue, *International Journal of Solids and Structures*, **47**, 2982-2990 (2010).
11. Z-S. Deng and J. Liu, Non-Fourier heat conduction effect on prediction of temperature transients and thermal stress in skin cryopreservation, *Journal of Thermal Stresses*, **26**, 7779-798 (2003).
12. J. Lin, Microwave Thermoelastic Tomography and Imaging, *Advances in Electromagnetic Fields in Living Systems*, **4**, 41-76 (2005)

8. Appendix

Table 1: Tissue parameters and constants

Parameter	Value	Reference
Geometrical Dimensions [mm]		
l_s	1.5	[6]
l_f	17	[6]
l_m	38	[6]
L	18.5	[6]
W	54.5	[6]
Permittivity		
ε_{skin}	1832.8	[6]
ε_{fat}	27.22	[6]
ε_{muscle}	1836.4	[6]
ε_{septa}	1832.8	Assumption
Electric conductivity [S/m]		
ω_s	2	[6]
ω_f	0.6	[6]
ω_m	0.5	[6]
Density [kg/m^3]		
ρ_s	1200	[6]
ρ_f	850	[6]
ρ_m	1270	[6]
ρ_{sp}	1200	Assumption
ρ_b	1000	[6]
Thermal conductivity [W/m/K]		
k_s	0.53	[6]
k_f	0.16	[6]
k_m	0.53	[6]
k_{sp}	0.53	Assumption
Specific heat [J/kg/K]		
c_s	3800	[6]
c_f	2300	[6]
c_m	3800	[6]
c_{sp}	3800	Assumption
c_b	3800	[6]
Young's Modulus [kPa]		
E_s	35	[9]
E_f	2	[9]
E_m	80	[9]
E_{sp}	0.009	[10]
Thermal expansion coefficient [1/^{o}C]		
α_s	6E-5	[11]
α_f	2.76E-5	[12]
α_m	4.14E-5	[12]
α_{sp}	6E-5	Assumption
Fixed constants		
h	10 [W/m^2/K]	
T_∞	298 [K]	
T_b	310 [K]	
T_{core}	310[K]	
T_{plate}	303[K]	